


COMMUNICATION

Recordings from neuron–HEK cell cocultures reveal the determinants of miniature excitatory postsynaptic currents

Chung-Wei Chiang, Wen-Chi Shu, Jun Wan, Beth A. Weaver, and Meyer B. Jackson 

Spontaneous exocytosis of single synaptic vesicles generates miniature synaptic currents, which provide a window into the dynamic control of synaptic transmission. To resolve the impact of different factors on the dynamics and variability of synaptic transmission, we recorded miniature excitatory postsynaptic currents (mEPSCs) from cocultures of mouse hippocampal neurons with HEK cells expressing the postsynaptic proteins GluA2, neuroligin 1, PSD-95, and stargazin. Synapses between neurons and these heterologous cells have a molecularly defined postsynaptic apparatus, while the compact morphology of HEK cells eliminates the distorting effect of dendritic filtering. HEK cells in coculture produced mEPSCs with a higher frequency, larger amplitude, and more rapid rise and decay than neurons from the same culture. However, mEPSC area indicated that nerve terminals in synapses with both neurons and HEK cells release similar populations of vesicles. Modulation by the glutamate receptor ligand aniracetam revealed receptor contributions to mEPSC shape. Dendritic cable effects account for the slower mEPSC rise in neurons, whereas the slower decay also depends on other factors. Lastly, expression of synaptobrevin transmembrane domain mutants in neurons slowed the rise of HEK cell mEPSCs, thus revealing the impact of synaptic fusion pores. In summary, we show that cocultures of neurons with heterologous cells provide a geometrically simplified and molecularly defined system to investigate the time course of synaptic transmission and to resolve the contribution of vesicles, fusion pores, dendrites, and receptors to this process.

Introduction

Synaptic transmission proceeds through a sequence of steps, beginning with presynaptic Ca^{2+} entry, followed by Ca^{2+} sensor activation, fusion pore opening, neurotransmitter diffusion into and across the synaptic cleft, postsynaptic receptor activation, local depolarization, and finally electrotonic spread of dendritic voltage changes to the cell soma (Sabatini and Regehr, 1999; Lisman et al., 2007). These steps are generally quite rapid, with sub-millisecond kinetics, and they all can impact the nature of a synaptic response. This makes it quite challenging to test the contributions of specific molecules and extract information about individual steps. One of these steps, neurotransmitter flux through a fusion pore, tracks the progress of membrane fusion, and modeling studies indicate that the pore must expand rapidly to produce transmitter concentrations high enough to activate synaptic receptors (Khanin et al., 1994; Clements, 1996; Stiles et al., 1996). In endocrine secretion, fusion pore flux can be measured directly with amperometry recording (Lindau and Alvarez de Toledo, 2003; Chang et al., 2017), but the complicated

sequential nature of synaptic transmission makes synaptic fusion pores more difficult to study.

One can simplify this problem by focusing on unitary, quantal events produced by the spontaneous exocytosis of single vesicles. These miniature excitatory postsynaptic currents (mEPSCs) bypass the upstream steps involving Ca^{2+} entry and triggering. However, a number of downstream steps remain, and mEPSCs introduce a new difficulty because of their high variance (Finch et al., 1990; Bekkers, 1994). Factors contributing to this variance may include receptor density and subunit composition, vesicle size, intravesicular transmitter concentration, pre- and postsynaptic apparatus registration, auxiliary proteins, and electrotonic distance (Bekkers et al., 1990; Lomeli et al., 1994; Geiger et al., 1995; Wu et al., 2007). Electrotonic distance is especially likely to obscure fusion pore effects because it slows the mEPSC onset, which depends critically on fusion pore size. Thus, it is difficult to use mEPSCs to investigate the function of exocytotic proteins in

Department of Neuroscience, University of Wisconsin School of Medicine and Public Health, Madison, WI.

Correspondence to Meyer B. Jackson: Meyer.Jackson@Wisc.Edu; C.-W. Chiang's present address is Department of Neuroscience, Baylor College of Medicine, Houston, TX; J. Wan's and B.A. Weaver's present address is Departments of Cell and Regenerative Biology and Oncology, Carbone Cancer Center, University of Wisconsin, Madison, WI.

© 2021 Chiang et al. This article is distributed under the terms of an Attribution–Noncommercial–Share Alike–No Mirror Sites license for the first six months after the publication date (see <http://www.rupress.org/terms/>). After six months it is available under a Creative Commons License (Attribution–Noncommercial–Share Alike 4.0 International license, as described at <https://creativecommons.org/licenses/by-nc-sa/4.0/>).

synapses, and only a few studies have successfully demonstrated that presynaptic molecular manipulations can alter quantal release (Pawlu et al., 2004; Guzman et al., 2010; Bao et al., 2018; Chiang et al., 2018).

To resolve the various contributions to quantal synaptic release, we have investigated mEPSCs in synapses formed by neurons on heterologous human embryonic kidney 293 (HEK 293) cells. Neuronal-HEK cell cocultures had been developed to assay specific postsynaptic receptor subunits in a synaptic context (Fu et al., 2003; Dixon et al., 2015) and to evaluate cell adhesion molecules in synaptogenesis (Sara et al., 2005; Dong et al., 2007). Synapses will form on HEK cells provided that they express the appropriate postsynaptic proteins. Expression of a synaptic receptor enables a nonneuronal cell to respond to a neurotransmitter such as glutamate. Neuroligins, which complex with neuexins from nerve terminals, recruit excitatory and inhibitory synaptic inputs to nonneuronal cells (Scheiffele et al., 2000; Dean et al., 2003; Dean and Dresbach, 2006). Neuroligins also recruit glutamate receptors into postsynaptic clusters through interactions with PSD-95 and stargazin (TARP $\gamma 2$; Chen et al., 2000; Schnell et al., 2002; Dean and Dresbach, 2006). HEK cells expressing neuroligin 1, PSD-95, and NMDA receptors (NR1-1a/NR2A) or α -amino-3-hydroxy-5-methyl-4-isoxazolepropionic acid (AMPA) receptors (GluA4) recruit synaptic inputs from cerebellar neurons to produce robust mEPSC activity as well as synaptic release evoked by Mg^{2+} (Fu et al., 2003). HEK cells expressing either neuroligin 1 or SynCAM (synaptic cell adhesion molecule) with GluA2 recruit synaptic inputs from hippocampal neurons, producing mEPSCs and synaptic responses evoked by high K^+ (Biederer et al., 2002; Sara et al., 2005). HEK cells expressing neuroligin-2 and γ -aminobutyric acid A ($GABA_A$) receptors recruit inhibitory synaptic inputs from hypothalamic neurons to produce miniature inhibitory postsynaptic currents and synaptic responses to action potentials (Dong et al., 2007). Neuroligin 1 and PSD-95 colocalize with the presynaptic protein synapsin in cerebellar-HEK cell cocultures (Fu et al., 2003), and nerve terminals cluster around glutamate receptors expressed in HEK cells in heterologous synapses (Biederer et al., 2002). In addition to permitting precise molecular control of the postsynaptic apparatus, the compact shape of HEK cells eliminates electrotonic distortion. This should mitigate significant sources of variance.

Here, we investigated synapses between mouse hippocampal neurons and HEK cells expressing the GluA2 AMPA-type glutamate receptor subunit, neuroligin 1, and PSD-95. In addition to these molecules employed by Fu et al. (2003), we also included stargazin, which improves receptor targeting (Chen et al., 2000). Detailed comparisons highlighted various contributions to the shapes of mEPSCs. Fusion pore perturbation with synaptobrevin harboring mutations in its transmembrane domain recapitulated changes seen in mEPSCs produced by synapses between neurons (Chiang et al., 2018), thus supporting a role for SNARE protein transmembrane domains in synaptic fusion pores. These studies of mEPSCs in neuron-HEK cell cocultures permit a dissection of the roles of diverse molecular determinants of quantal synaptic release.

Materials and methods

Molecular biology

DNA constructs encoding neuroligin 1 (harboring a hemagglutinin tag), stargazin-GFP (TARP $\gamma 2$ fused with GFP), PSD-95, and GFP-GluA2 (GFP fused with the AMPA receptor subunit GluA2) separated by internal ribosome entry site elements were provided by Dr. Lu Chen (Stanford University, Stanford, CA). To provide a separate fluorescence channel, mCherry was subcloned into the GluA2 construct in place of enhanced GFP. PCR was used with a forward primer containing the signaling peptide sequence. The P2A sequence was introduced to replace the internal ribosome entry site using PCR and Gibson assembly. Neuroligin 1-P2A-stargazin-GFP and PSD-95-P2A-mCherry-GluA2 were then subcloned into a retroviral vector driven by a cytomegalovirus promoter containing hygromycin B and puromycin resistance gene cassettes, respectively, for antibiotic selection.

Hippocampal neuron and HEK cell coculture

Hippocampal neurons were cultured from embryonic E17.5–18.5 WT C57BL/6 mice. The hippocampus was dissected and dissociated with 0.05% (wt/vol) trypsin-EDTA. Cells were plated at a density of $80\text{--}120 \times 10^3$ per well onto 12-mm #1 coverslips coated with 0.2 mg/ml poly-D-lysine (borate buffer, pH 8.5, overnight) in 24-well plates. Neurons were incubated at 37°C with 5% CO_2 /air in Neurobasal plus culture medium supplemented with GlutaMAX-I, B27 plus, and ampicillin/streptomycin. AraC (1.5 μM) was added at 2–3 d in vitro (DIV) to reduce glial cell growth. Half the medium was replaced every 3–4 d for the first 2 wk and every 2 d after 16–17 DIV.

HEK 293T cells (from American Type Culture Collection; product #ATCC CRL-3216) were passaged twice a week up to 32 times. Cells in six-well plates were transfected with the above-described neuroligin 1-P2A-stargazin-GFP and PSD-95-P2A-mCherry-GluA2 constructs using calcium phosphate or X-tremeGENE HP (Merck Millipore). Cells were incubated with serum-free opti-MEM (Gibco) during transfection. Medium was switched back to Dulbecco's modified Eagle's medium with 10% FBS after 4–6 h. After another 18 h, the cells were digested with 0.05% (wt/vol) trypsin-EDTA and resuspended with the same Neurobasal culture medium used for hippocampal neurons. Cells were added directly to the coverslips (15×10^3 cells/well) with neurons at either 13–14 DIV or 17–18 DIV. GFP and mCherry fluorescence were used to find HEK cells expressing both constructs for patch clamp recordings.

Electrophysiology

Whole-cell patch clamp recording was performed between 1 and 3 d after plating HEK cells for coculture. We recorded from both neurons and double-fluorescent HEK cells in the same cultures. An Axopatch 200B (Molecular Devices) amplifier controlled by pClamp 10 (Molecular Devices) was used to acquire one to four 1-min gap-free recordings. Coverslips with cocultured cells were transferred to 35-mm dishes containing extracellular solution consisting of (in mM) 140 NaCl, 5 KCl, 5 CaCl_2 , 1 MgCl_2 , 10 HEPES, and 10 glucose (pH 7.4 at room temperature). Note that 5 mM of calcium increases mEPSC frequency and facilitates their study (Scanziani et al., 1992; Bekkers and Stevens, 1995;

Chiang et al., 2018). NMDA receptors, γ -aminobutyric acid receptors, and action potentials were blocked with 50 μ M amino phosphonovaleric acid, 10 μ M SR95531, and 0.5 μ M tetrodotoxin, respectively. Aniracetam was added to the extracellular solution for the indicated experiments. Patch pipettes (3–7 M Ω when filled) were pulled with Narishige PC-10 puller. After coating with Sylgard, the pipettes were filled with intracellular solution consisting of (in mM) 120 Cs-gluconate, 8 CsCl, 2 NaCl, 10 EGTA, 5 phosphocreatine, 5 HEPES, 2 Mg-ATP, and 0.3 Na-GTP. Membrane potential was held at –65 mV throughout recordings. Series resistance was compensated >75%, and cells with series resistance >20 M Ω before compensation were discarded.

Data analysis and statistics

Raw pClamp traces were imported into IGOR Pro (WaveMetrics) with the aid of NeuroMatic (Rothman and Silver, 2018) for analysis with custom programs used in previous studies (Chiang et al., 2018). Individual mEPSCs were identified by a threshold criterion and fitted (by χ^2 minimization) to the following function with an exponential rise and decay:

$$I(t) = A \cdot \left(1 - e^{-t/\tau_1}\right) \left(e^{-t/\tau_2}\right). \quad (1)$$

The parameters from fits were used to calculate amplitude, area, decay time, rise rate, and 10–90% rise time. The rise rate was the maximal slope of the rising phase divided by amplitude to give a quantity independent of amplitude. All statistical analysis was performed with Origin Pro (OriginLab). The two-sample *t* test was used for hypothesis testing if not specified otherwise. Asterisks indicate significance at the following levels: *, *P* < 0.05; **, *P* < 0.01; and ***, *P* < 0.001. All *P* values are presented in the figure legends, and some are stated in the text as well where appropriate to the discussion.

Results

A postsynaptic neuron presents a variety of diverse sites for presynaptic input, including dendritic shafts, spines, and somata. Dendritic inputs can range from proximal to distal locations, and distal synapses elicit slower voltage changes at the soma compared with proximal synapses (Rall, 1967; Rall et al., 1967; Jack and Redman, 1971; Rall, 1989). Thus, with synapses between neurons, variations in this distance can impact electrotonic conduction, making mEPSCs more variable. HEK cells lack these processes and present uniform sites for synaptic inputs. The resulting close proximity between synaptic input and recording electrode eliminates electrotonic distortion. To induce synapse formation on HEK cells, we transfected them with four postsynaptic proteins described in Materials and methods and then cocultured them with hippocampal neurons.

Synapse formation with HEK cells

Patch clamp recordings from HEK cells demonstrated functional synaptic inputs from neurons in coculture. Cells were selected based on visual emission in both the red and green fluorescence channels to detect expression of the GluA2-mCherry-PSD-95

construct and the neuroligin 1–stargazin-GFP construct, respectively. Recordings from cells with fluorescence in only one channel never produced mEPSCs. In HEK cells cocultured with 14-DIV neurons, recordings 1–4 d later revealed very little mEPSC activity (Fig. 1 A). Only 4 out of 58 cells produced mEPSCs (7%), and the frequency was very low (Fig. 1 B; cell numbers given at base of bars). This indicated that neurons at this stage either fail to innervate HEK cells or their synapses are not functional. Increasing the plating density of neurons from 80–120K to 120–150K (per coverslip) failed to increase the mEPSC frequency. By contrast, in cocultures with 17-DIV neurons, patch clamp recordings from HEK cells the next day (at 18 DIV) revealed robust mEPSC activity at a frequency of 4.3 ± 0.77 Hz (Fig. 1, A and B) in 24 out of 39 cells (61%; Fig. 1 B; cells with zero mEPSCs not included in frequency average). Recordings from neurons in these cocultures revealed mEPSCs at both 14 and 18 DIV (Fig. 1 A), with a similar frequency of ~ 1.3 Hz in both. This frequency was approximately threefold lower than in HEK cells from 18-DIV cocultures (Fig. 1 B). Because mEPSCs were much more robust in HEK cells with 18-DIV neurons, we used these cocultures for further study.

mEPSC properties

Individual mEPSCs recorded from both neurons and HEK cells were generally well fitted by a function with an exponential rise and decay (Eq. 1 in Materials and methods; Fig. 2 A). The averages computed from the pooled events revealed striking differences, with mEPSCs in HEK cells being larger and faster than those in neurons (Fig. 2 B). To explore these differences in detail, the parameters obtained from fits to Eq. 1 were used to calculate the peak amplitude, area, decay time, 10–90% rise time, and maximum rise rate for each event. Fig. 2 C presents the means for these quantities, with standard errors (based on cell number, stated in bars for amplitude). The amplitude and area showed modest $\sim 25\%$ increases between neurons at 14 and 18 DIV, but the kinetic parameters were all indistinguishable between the two age groups (Fig. 2 C). mEPSCs in HEK cells had significantly larger amplitudes, but the areas were similar. As apparent from the comparison of plotted mEPSC averages (Fig. 2 B), mean mEPSC rises and decays were more rapid in HEK cells than in neurons (Fig. 2 C). The similar areas, larger amplitudes, and more rapid kinetics in HEK cell mEPSCs are consistent with the elimination of electrotonic conduction. The similar areas suggest that a synaptic input gates the entry of similar amounts of charge at synapses in both neurons and HEK cells. The different kinetic parameters could reflect either more dendritic filtering in neurons or differences in receptor function; dendritic filtering will be examined below.

mEPSC variability

To focus on mEPSC variability, we plotted the coefficient of variation (CV; Fig. 2 D). All mEPSC parameters had greater variation in neurons at 18 DIV than at 14 DIV (Fig. 2 D), as expected for the greater morphological complexity of older neurons (the plating densities were the same). Although HEK cells present more uniform locations for synapse formation, the amplitude and decay time had significantly higher CVs in HEK

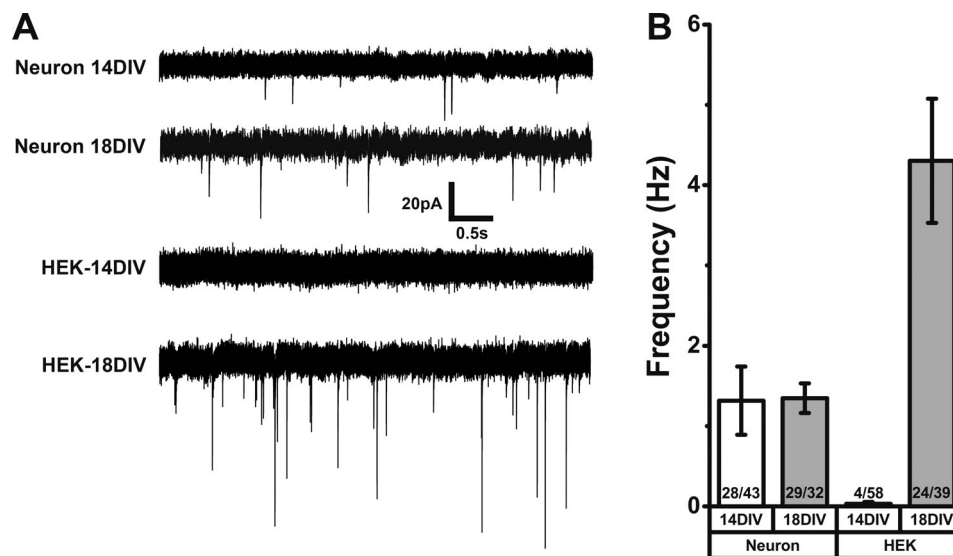


Figure 1. **mEPSCs in neurons and HEK cells.** (A) Sample traces from HEK cells cocultured with 14-DIV and 18-DIV neurons reveal mEPSCs in neurons at both ages, but in HEK cells mEPSCs are only robust in cocultures with 18-DIV neurons. (B) Average mEPSC frequencies from cocultures of HEK cells with 14-DIV and 18-DIV neurons, plated at equal densities (number of cells with mEPSCs/number of cells recorded in each bar). Error bars represent SEM.

cells than in neurons (Fig. 2 D). The amplitude CV was 0.50 ± 0.02 for neurons versus 0.62 ± 0.02 for HEK cells (two-sample *t* test, $t = 3.27$, $P = 0.0019$), while the CV for decay was 0.38 ± 0.01 for neurons and 0.50 ± 0.04 for HEK cells (two-sample *t* test, $t = 3.21$, $P = 0.0023$). This indicates that neuronal synapses have other sources of variation in addition to electrotonic distance and molecular composition. Since the only excitatory receptor subunit in the HEK cells is GluA2, the variability in their mEPSCs cannot be attributed to heterogeneity of subunit composition. Nonuniform receptor density is a likely source of variance, and this could arise from variable expression levels of any of the transfected proteins. They can all influence receptor density, as well as receptor recruitment to synaptic contacts. Furthermore, stargazin modulates glutamate receptors (Priel et al., 2005; Tomita et al., 2005; Zhang et al., 2006; Carrillo et al., 2020), and its expression levels could influence mEPSC amplitude and shape.

The CV for area and 10–90% rise times did not differ significantly between neurons and HEK cells (Fig. 2 D). Interestingly, the mEPSC rise rate was not only faster in HEK cells than in neurons but also less variable. The rise rate does not depend on receptor density, so this lower variation may reflect uniformly proximal electrotonic locations of the synaptic inputs in HEK cells. Since the maximum rise rate depends in part on fusion pore size, the reduced variance suggests that mEPSCs in HEK cells may provide a better way to assess synaptic fusion pore function. Since maximum rise rate reflects the earliest and most rapid phase of mEPSC onset, we focused on this quantity and omitted 10–90% rise times from further analysis.

To examine variations in greater detail, we plotted cumulative distributions of mEPSC amplitude (Fig. 3 A), area (Fig. 3 B), decay time (Fig. 3 C), and rise rate (Fig. 3 D). The shifts in distributions of amplitude, decay, and rise rate between neurons and HEK cells are consistent with the differences in mean (Fig. 2

C) and indicate that these differences reflect overall changes across the population rather than changes in the proportions of distinct subsets of mEPSCs. The distributions of area were very similar (Fig. 3 B), and we examined mEPSC area more closely in an attempt to evaluate the vesicle populations for synapses on neurons and HEK cells. Assuming a constant intravesicular glutamate concentration that does not vary between vesicles of different sizes and further assuming a proportional relation between the number of glutamate receptors activated and the number of molecules of glutamate released should result in a scaling relation between vesicle volume and mEPSC area.

Since volume is proportional to diameter cubed, we examined the distribution of the cube root of mEPSC area. In both HEK cells (Fig. 3 E) and neurons (Fig. 3 F), these distributions had a similar appearance, with main peaks at similar values and shoulders on the right. These distributions were well fitted by a sum of two Gaussians with similar parameters (see legend of Fig. 3). Interestingly, the second peak was located at a value of $(\text{area})^{1/3}$ that was 39% higher than the first peak for HEK cells and 32% higher than the first peak for neurons. The second peak has 67% of the events in the first peak in the HEK cell distribution and 51% of the events in the first peak in the neuron distribution. Taking the cube of the ratios of the positions of the peaks suggests that the larger population of vesicles has 2.69 times more glutamate molecules in neuron-HEK cell synapses and 2.30 times more glutamate molecules in neuron-neuron synapses. Thus, the larger population of vesicles may result from the fusion of two smaller vesicles. The similar distributions of $(\text{area})^{1/3}$ in Fig. 3, E and F support the interpretation that similar populations of vesicles are released at both neuron-neuron and neuron-HEK cell synapses. Thus, in terms of vesicle size, hippocampal nerve terminals function similarly in their targeting of neuronal and nonneuronal cells; the

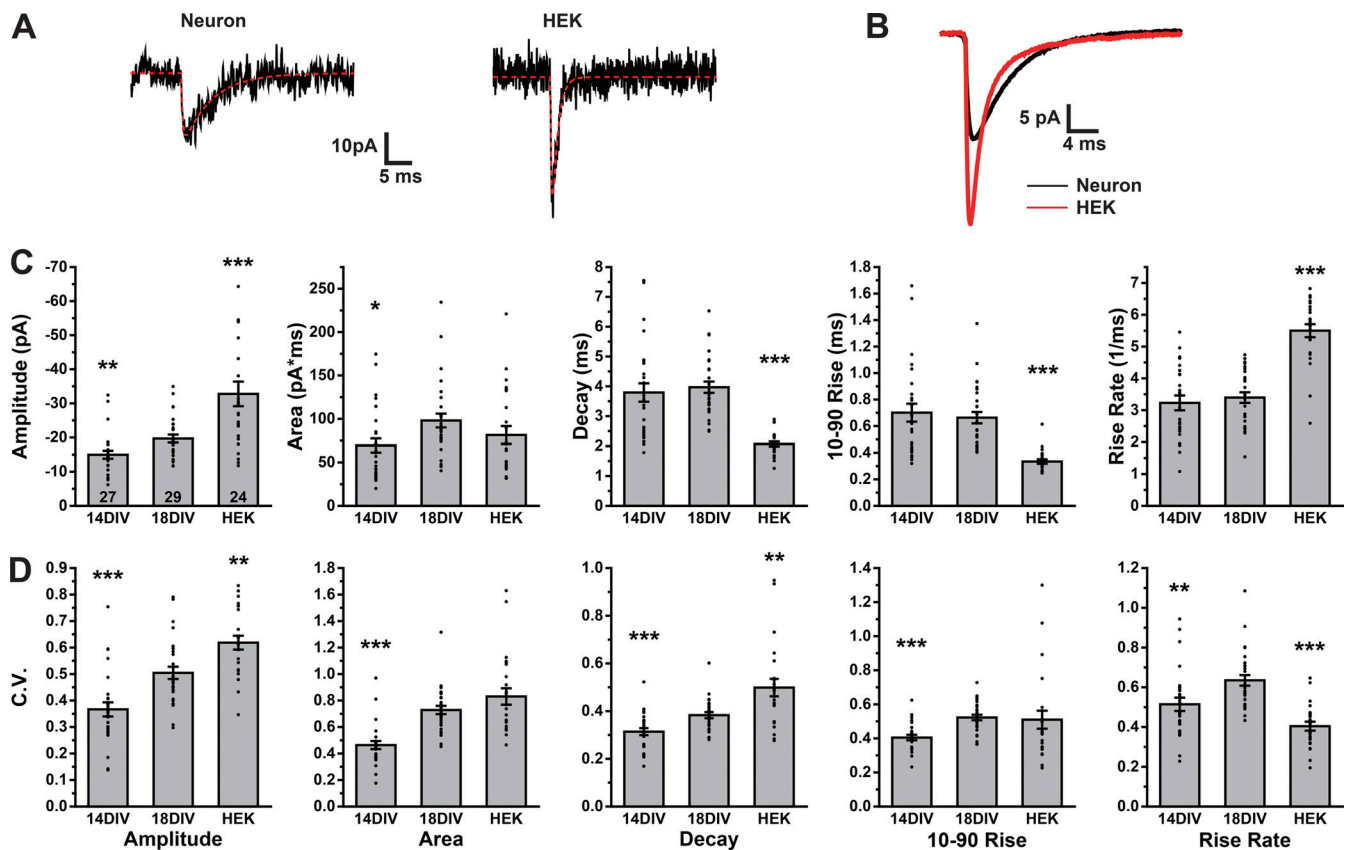


Figure 2. mEPSC properties and variance in neurons and HEK cells. (A) mEPSCs recorded from a neuron and a HEK cell illustrating the fit to Eq. 1 as light red dashed curves. (B) The average of all mEPSCs recorded from 18-DIV neurons (black; 3,170 events) and HEK cells (red; 2,715 events). (C) Mean values of parameters obtained from fits to Eq. 1 from 14-DIV neurons, 18-DIV neurons, and HEK cells. Amplitude, total area, decay time, 10–90 rise time, and maximum rise rate were calculated for each event from fits as in A. Cell means are plotted using cell number (stated in amplitude bars) to calculate standard error. P values for statistical significance are 0.00604 (amplitude: 14 DIV versus 18 DIV), 0.00049 (amplitude: HEK versus 18 DIV); 0.0015 (area: 14 DIV versus 18 DIV), 0.20 (area: HEK versus 18 DIV); 0.62 (decay: 14 DIV versus 18 DIV), $<10^{-5}$ (decay: HEK versus 18 DIV); 0.64 (rise time: 14 DIV versus 18 DIV), $<10^{-5}$ (rise time: HEK versus 18 DIV); 0.558 (rise rate: 14 DIV versus 18 DIV), and 10^{-5} (rise rate: HEK versus 18 DIV). *, $P < 0.05$; **, $P < 0.01$; ***, $P < 0.001$. (D) CVs for the quantities plotted in C. CVs were averaged across cells, and errors were based on cell number. P values for statistical significance are 0.00025 (amplitude: 14 DIV versus 18 DIV), 0.00194 (amplitude: HEK versus 18 DIV); $<10^{-5}$ (area: 14 DIV versus 18 DIV), 0.129 (area: HEK versus 18 DIV); 0.00075 (decay: 14 DIV versus 18 DIV), 0.0023 (decay: HEK versus 18 DIV); $<10^{-5}$ (rise time: 14 DIV versus 18 DIV), <0.80 (rise time: HEK versus 18 DIV); 0.00642 (rise rate: 14 DIV versus 18 DIV), and 0.0004 (rise rate: HEK versus 18 DIV). **, $P < 0.01$; ***, $P < 0.001$. Error bars represent SEM.

postsynaptic target does not impact the size of the vesicles in the innervating terminal. Thus, the differences between mEPSCs in the two cell types are likely to reflect postsynaptic components.

Cable analysis

The lower amplitude, slower rise, and slower decay of mEPSCs in neurons compared with HEK cells (Fig. 2 C) could reflect the impact of electrotonic conduction from the site of a dendritic input to the soma. However, the locations of dendritic inputs, and therefore the electrotonic distances, should vary to make the CVs greater in neurons. The CV for the rise rate was in fact higher in neurons, but the CVs for amplitude and decay were lower (Fig. 2 D). We investigated the potential impact of dendritic filtering further using cable theory to model electrotonic conduction. First, we took the average mEPSCs from HEK cells and neurons from Fig. 2 B and normalized them to highlight the slower time course in neurons (Fig. 4 A). The impact of electrotonic distance can be evaluated with the aid of the Rall model of a neuron in which the dendrite is represented as an

equivalent cylinder (Rall, 1967; Rall et al., 1967; Jack and Redman, 1971; Rall, 1989). For a voltage-clamped soma with a cylindrical dendrite of electrotonic length L with a sealed end, a synaptic input with a local effect of $v(t)$ at an electrotonic distance X (between 0 and L) will give rise to a voltage change at the soma, $V(t)$, of the form

$$V(t) = \int_0^t 2 \sum_{n=1}^{\infty} \alpha_n \sin(\alpha_n X) e^{-\frac{(1+\alpha_n^2)(t-s)}{\tau_m}} v(t) ds, \quad (2)$$

where $\alpha_n = (2n - 1)\pi/2L$; τ_m , the membrane time constant, was taken as 10 ms. Eq. 2 is the convolution integral of $v(t)$ with the impulse response computed from the solution to the cable equation (Rall, 1969; Jackson, 2006).

The local input, $v(t)$, can be taken as the average mEPSC recorded in HEK cells (Fig. 4 A). This response is not distorted by dendritic filtering, and the cable model will aid in determining whether the difference between neurons and HEK cells displayed in Fig. 4 A reflects dendritic filtering or other factors. We

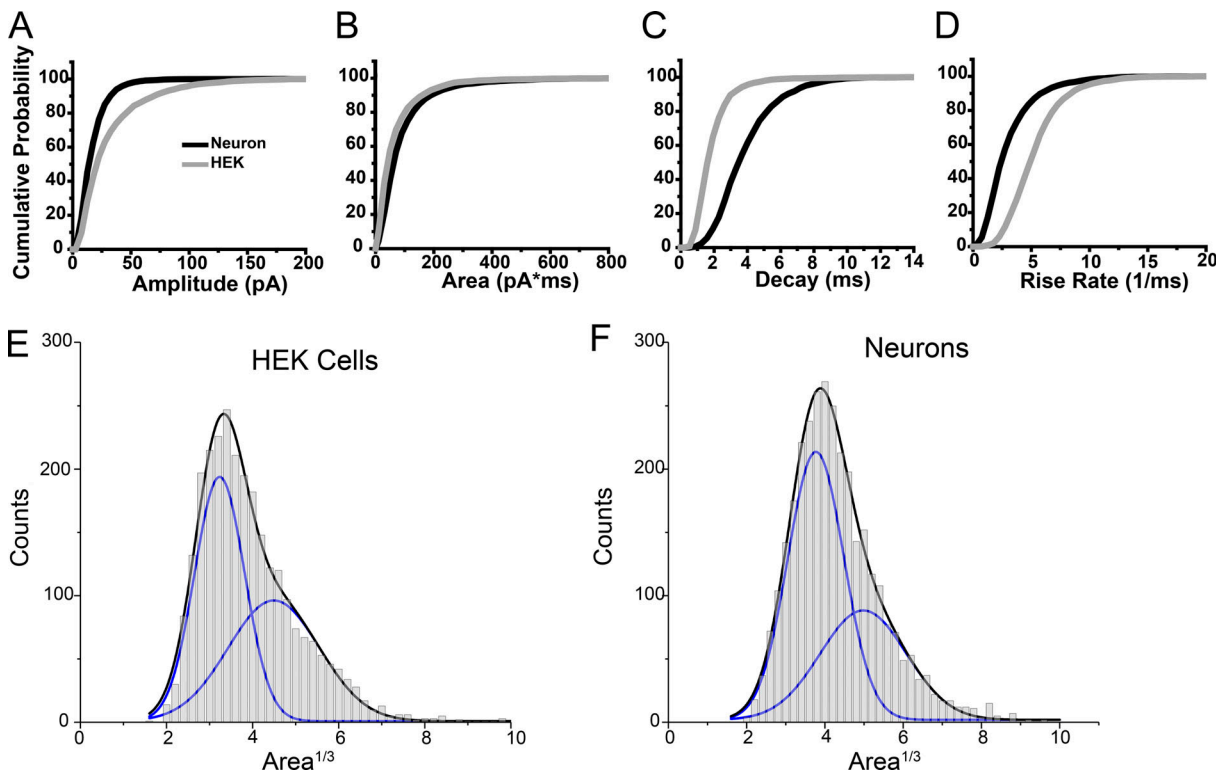


Figure 3. **mEPSC distributions in neurons and HEK cells.** (A–D) Cumulative distributions of amplitude (A), area (B), decay time (C), and rise time (D) for mEPSCs recorded from neurons (black) and HEK cells (gray). (E and F) The areas from B were transformed to $(\text{area})^{1/3}$, and the numbers per bin were plotted for HEK cells (E) and neurons (F). Both distributions were well fitted by a sum of two Gaussians. For HEK cells: peak 1, height = 193, center = 3.23, width = 1.16; peak 2, height = 95, center = 4.49, width = 2.12. For neurons: peak 1, height = 212, center 3.77, width = 1.43; peak 2, height = 86, center = 4.98, width = 2.20. Black curves are the best-fitting sum of two Gaussians and blue curves are the individual Gaussian terms.

used the following empirical expression to represent the average HEK cell mEPSC:

$$v(t) = (1 - e^{-\frac{t}{\tau_1}}) \left(A_1 e^{-\frac{t}{\tau_2}} + A_2 e^{-\frac{t}{\tau_3}} \right). \quad (3)$$

Fig. 4 A shows that a plot of this expression (red trace) overlies the average HEK cell mEPSC (black trace) with no perceptible

discrepancies (see the legend of Fig. 4 for the parameters for Eq. 3). The voltages at the soma for an electrotonically filtered mEPSC were computed by using this expression for $v(t)$ in Eq. 2. The results are plotted for $L = 0.5$ (Fig. 4 B) and $L = 1$ (Fig. 4 C), with various input distances, X , to illustrate the range of responses. Fig. 4, B and C also replot the average mEPSC of neurons from Fig. 4 A for comparison with the simulations. We see

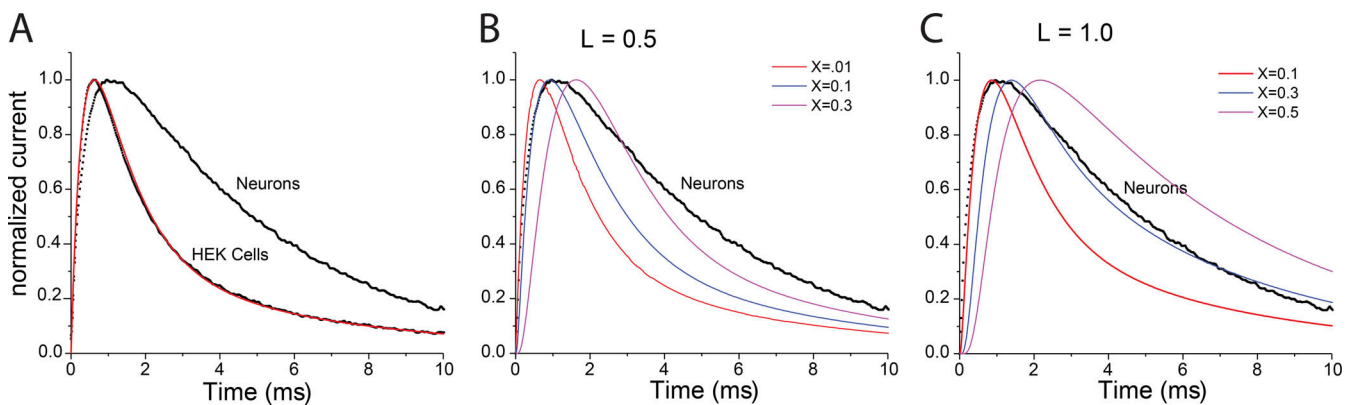


Figure 4. **Cable analysis of mEPSCs.** (A) Average of all mEPSCs from neurons and HEK cells (from Fig. 2 B) were normalized. Eq. 3 was fitted to the HEK cell trace (red; $\tau_1 = 0.428$ ms; $\tau_2 = 1.13$ ms; $\tau_3 = 6.16$ ms; $A_1 / (A_1 + A_2) = 0.825$). Cable effects on averaged mEPSCs were simulated with Eq. 2, taking $v(t)$ from the fit of Eq. 3. (B) Simulations of mEPSCs with $L = 0.5$ and the indicated positions of the synaptic inputs (X). (C) Simulations of mEPSCs with $L = 1.0$ and indicated values of X . The same average mEPSC from neurons was replotted in B and C as a black line.

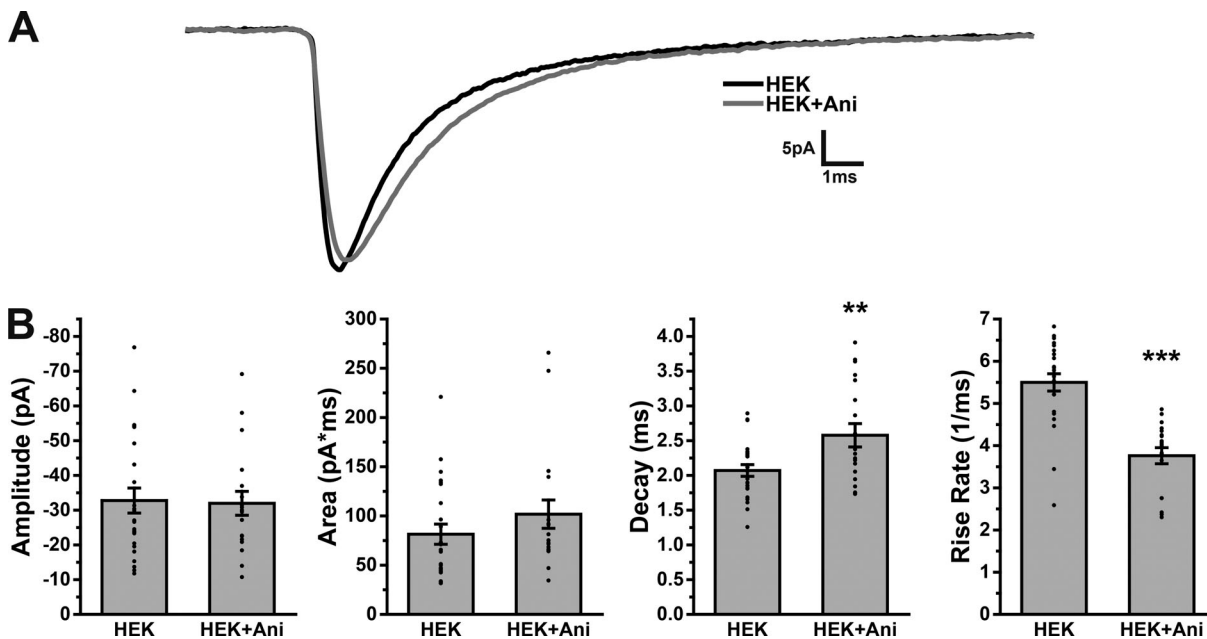


Figure 5. **Drug effects on mEPSCs in HEK cells.** (A) The average control mEPSC is plotted with the average in aniracetam (Ani). (B) Means \pm standard errors are plotted for amplitude, area, decay time, and rise rate for mEPSCs recorded in HEK cells with and without aniracetam. For decay times, $P = 0.0063$, and for rise rates, $P < 10^{-5}$ for Ani versus control. **, $P < 0.01$; ***, $P < 0.001$.

that for $L = 0.5$, moving the input out from $X = 0.01$ through 0.5 prolongs the rise of the computed mEPSC with very little change in the decay phase, presumably because $L = 0.5$ is too compact. For $L = 1$, moving the input from 0.1 through 0.5 does generate slower decays, but for $X = 0.5$, where the decay is comparable to that of the neuronal mEPSC, the rise is much slower. For both $L = 0.5$ and 1.0, the rise of the neuronal mEPSC was accurately reproduced using $X = 0.1$, but the decay was too fast in both cases. The overall closest simulation was seen with $X = 0.3$ and $L = 1$, but $V(t)$ rose too slowly and decayed too rapidly. The neuronal mEPSC was thus not fully reconstructed by a model based on cable theory with the HEK mEPSC as input. Dendritic filtering can account for the slower mEPSC rise rate in neurons, but factors other than dendritic filtering must be invoked to interpret the difference in decay kinetics.

Receptor contributions

To evaluate the contributions of AMPA receptors to mEPSC shape, we tested aniracetam, a drug that binds to AMPA receptors and inhibits deactivation and desensitization (Ito et al., 1990; Isaacson and Nicoll, 1991; Vyklicky et al., 1991; Brenowitz and Trussell, 2001). In neuronal synapses, aniracetam increased mEPSC amplitudes by reducing ambient receptor inactivation (Lawrence et al., 2003). In mEPSCs recorded from HEK cells, we found that aniracetam (1 mM) left the amplitude and total area of mEPSCs unchanged but reduced the rates of mEPSC rise and decay (Fig. 5). These changes in kinetics were not seen in mEPSCs in cultured hippocampal neurons (Chiang et al., 2018). The differences in aniracetam actions are likely to reflect differences in pharmacological sensitivity of receptors formed by different glutamate receptor subunits (Johansen et al., 1995).

Aniracetam actions are very sensitive to the ambient levels of glutamate and to the residence time of glutamate in the synaptic cleft, so the difference between the actions on HEK cell mEPSCs versus neuronal mEPSCs could also indicate that their synapses differ in one or both of these respects.

Fusion pore contributions

To test the impact of fusion pores on mEPSCs in HEK cells, we transfected the hippocampal neurons with synaptobrevin 2 (Syb2) mutants harboring tryptophan in the transmembrane domain. These mutants had been tested previously for effects on mEPSCs in synapses between neurons (Chiang et al., 2018). For these experiments, we prepared neurons from Syb2/cellubrevin double-knockout mice, which have a very low background frequency of mEPSCs. This enabled us to view mEPSCs that depend on an expressed form of Syb2. Neurons were transfected by lentiviral infection at 14 DIV with WT and mutant Syb2. HEK cells were added 3 d later, and patch clamp recordings were made at 18 DIV. These cocultures were thus similar to those in our other 18-DIV experiments. mEPSCs recorded from HEK cells cocultured with neurons from double-knockout mice expressing WT Syb2 were indistinguishable from mEPSCs seen in HEK cells cocultured with neurons from WT mice (compare means for WT Syb2 in Fig. 6 with means for HEK cells in Fig. 2 C).

Expressing Syb2 mutants with tryptophan at position 101, 102, and both 101 and 103 (2W) had no significant effect compared with WT Syb2 on the amplitudes and areas of mEPSCs in cocultured HEK cells (Fig. 6, A and B). However, the 101 and 2W mutations both produced significant reductions in the mEPSC rise rate of $\sim 25\%$ (Fig. 6 C; 101W: $t = 3.57$, $P = 0.0021$; 2W: $t = 3.13$, $P = 0.0057$; two-sample t test). A statistically significant increase

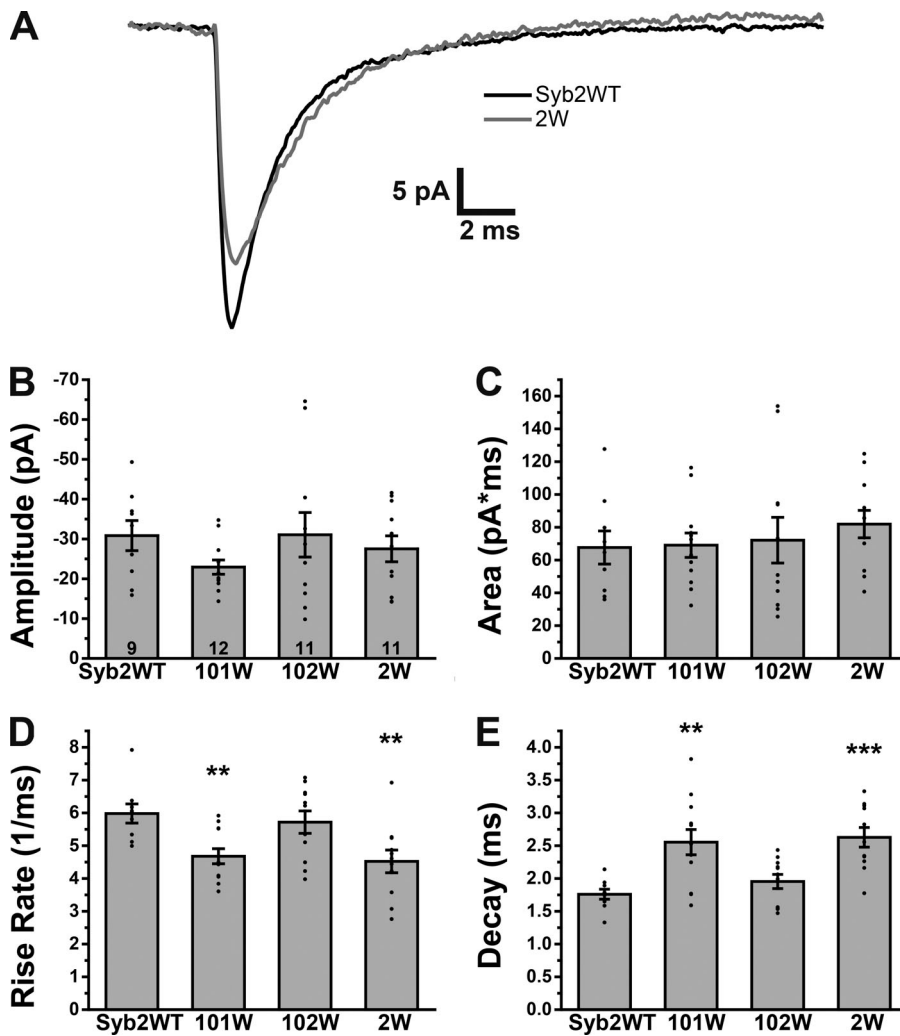


Figure 6. mEPSC recorded in HEK cells cultured with Syb2/cellubrevin knockout neurons transfected with WT-Syb2 and two Syb2 tryptophan TMD mutants. (A) Average of HEK cell mEPSCs with neurons expressing WT Syb2 (Syb2WT) and a Syb2 double mutant with tryptophan at positions 101 and 103 (2W). (B-E) Plots of amplitude (B), area (C), rise rate (D), and decay time (E) for the indicated mutants. Cell means \pm standard errors with cell numbers in the amplitude bars of B. For rise rate (D), $P = 0.0021$ for 101W versus WT and 0.0057 for 2W versus WT. For decay (E), $P = 0.003$ for 101W versus WT and 0.00014 for 2W versus WT. **, $P < 0.01$; ***, $P < 0.001$.

in the decay time of 45% was also observed with the 101 and 2W mutants (Fig. 6 D; two-sample t test, $t = 3.41$, $P = 0.0030$ and $t = 4.82$, $P = 1.4 \times 10^{-4}$, respectively). These mutants were previously shown to produce similar changes in mEPSCs of neuronal synapses (Chiang et al., 2018). The residue at position 102 is not a fusion pore liner (Chang et al., 2015; Chiang et al., 2018), and as reported previously with neuron-neuron synapses, this mutant did not change mEPSCs significantly in neuron-HEK cell synapses in any respect (Fig. 6). In neurons, the 2W double mutation was previously shown not to alter the mEPSC decay time (Chiang et al., 2018), but in HEK cells it did. Thus, HEK cells offer improved resolution of the impact of fusion pore perturbations on mEPSC shape, revealing clear and significant effects with data from half the number of cells.

Fusion pore modeling

To relate the changes that Syb2 mutants produced in mEPSCs to fusion pores, we adapted a model for fusion pore flux and receptor activation from a previous study of neuronal mEPSCs (Chiang et al., 2018). In this work, we had modeled the time course of synaptic cleft glutamate as the convolution of an exponential function with the solution of the diffusion equation in polar coordinates (Eq. 2 of Chiang et al., 2018):

$$N(t) = \frac{N_0}{4\pi D \tau_{fp}} \int_0^t \frac{e^{-s/\tau_{fp}}}{t-s} ds. \quad (4)$$

The exponential tracks the loss of glutamate from the vesicle through the fusion pore; the time constant, τ_{fp} , is inversely proportional to the fusion pore permeability. To model receptor activation in the present study with HEK cells expressing GluA2, we started with the kinetic scheme used previously (Fig. 7 A) but took the kinetic parameters for GluA2 flop GN expressed in HEK cells (Krampfl et al., 2002). As in our previous work in neurons (Chiang et al., 2018), the mEPSC decay was too rapid to be modeled with the complete set of published parameters, and this was corrected by reducing the channel closing rate constant, α , from 5 to 2.4 ms^{-1} . All the other parameters were from Krampfl et al. (2002) (Fig. 7 B). Even with this change, the fit to the model showed some deviations from the data. With $\tau_{fp} = 0.24 \text{ ms}$, we obtained a good fit to the rising phase, but the decay deviated somewhat (Fig. 7 C) due to the bi-exponential decay of the average mEPSC in HEK cells (Fig. 4 A and Eq. 3). The kinetic model produces mEPSCs dominated by a single exponential decay. This contrasts with fits to mEPSCs in neurons, where the relevant model fitted the average mEPSC essentially perfectly (Chiang et al., 2018). This discrepancy with the model in the present

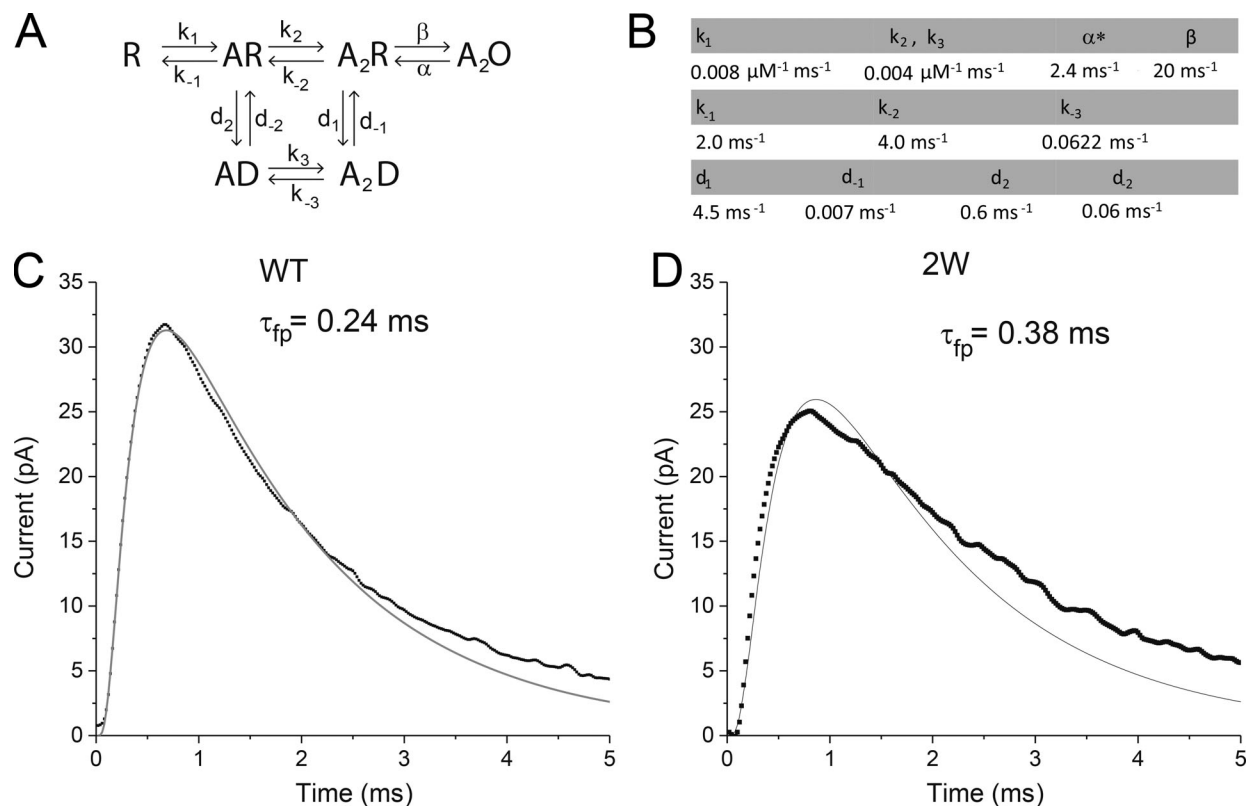


Figure 7. Simulations of mEPSCs based on fusion pore flux and the receptor model for GluA2 flop. Related to Krampfl et al., 2002. **(A)** Kinetic scheme illustrating receptor states (R), open (O), desensitized (D), and agonist (A). **(B)** Values of the rate constants of the various transitions in A. Asterisk indicates that the value of α was reduced from 5 ms^{-1} to the value displayed to fit the average mEPSC seen with WT Syb2. **(C)** The average mEPSC recorded from HEK cells cocultured with neurons expressing WT Syb2 and a simulation (gray) with a time constant for fusion pore flux (τ_{fp} ; Eq. 4) of 0.24 ms. **(D)** The average mEPSC recorded from HEK cells cocultured with neurons expressing the double Syb2 mutant (2W) and a simulation with $\tau_{fp} = 0.38 \text{ ms}$.

study probably reflects an influence of stargazin, which was present in our study but not in that of Krampfl et al. (2002) and is known to influence receptor kinetics (Priel et al., 2005; Tomita et al., 2005; Zhang et al., 2006; Carrillo et al., 2020).

Turning to the average mEPSC of the 2W domain mutant, we found that adjusting only the fusion pore parameter, τ_{fp} , to 0.38 ms successfully reproduced both the reduced amplitude and the slower rise time but worsened the fit to the decaying phase (Fig. 7 D). Despite the poor fit to the decay, it is nevertheless significant that adjusting a single parameter accounted for the changes in both the rise rate and amplitude. This suggests that the 2W mutation reduces glutamate flux through the synaptic vesicle fusion pore by 58%.

Discussion

mEPSCs recorded from neurons and cocultured HEK cells exhibited quantitative differences in their properties. The comparison provided insight into how synaptic transmission is influenced by a variety of molecular and cellular controls. Differences between mEPSCs, some of which were subtle, revealed the distinct roles of vesicles, receptors, dendrites, and fusion pores in shaping synaptic transmission. The elimination of electrotonic distortion in the postsynaptic HEK cells of these cocultures provides an experimental system with significant

advantages for biophysical studies of mEPSCs, providing improved resolution over cultured neurons. The defined molecular composition of the postsynaptic apparatus represents another advantage. It will be important to extend the study of homomeric GluA2 receptors presented here to naturally occurring heteromeric glutamate receptors. This will depend on how readily the palette of expressed molecules can be expanded beyond the four proteins expressed in the present work. The developmental state of the synapses in this system remains unclear. Although these synapses release spontaneously, a test of evoked release will be necessary for a full comparison with native synapses between neurons. The structural organization of the postsynaptic apparatus in heterologous cells has not been investigated, and comparisons with native synapses will be enhanced by super-resolution imaging studies of synapses on heterologous cells.

Synaptogenesis

This study showed that mouse hippocampal neurons formed functional synapses with HEK cells expressing GluA2, neuroigin 1, PSD-95, and stargazin. These four proteins thus support robust postsynaptic function, but their sufficiency cannot be judged because HEK cells express additional proteins that could contribute (Inada et al., 2016). We found that 18-DIV neurons formed synapses on HEK cells, but 14-DIV neurons did not, even

with a higher plating density. Neurons at 14 DIV formed synapses with one another and produced mEPSCs at the same frequency as 18-DIV neurons. Synaptogenesis between 14-DIV neurons may involve signaling molecules not recognized by the neuroligin 1 we expressed in HEK cells. It is also possible that the release at synapses on HEK cells arises from more mature synapses with a larger reserve pool of vesicles (Mozhayeva et al., 2002; Andreae et al., 2012). We observed an mEPSC frequency, amplitude, and decay time in HEK cells similar to those reported by Fu et al. (2003), who used HEK cells expressing the proteins we used except for their omission of stargazin. The mEPSC frequency in our HEK cells was approximately threefold higher than in both 14- and 18-DIV neurons (Fig. 1 B). HEK cells, despite their smaller surface area and lack of dendrites, could conceivably present more sites receptive to innervation, but individual synaptic contacts on HEK cells could also release more vigorously. Previous work on synapses in HEK cells expressing the adhesion molecule SynCAM and the AMPA receptor GluA2 cocultured with hippocampal neurons reported mEPSCs in 30% of the heterologous cells (Biederer et al., 2002) with slightly smaller amplitudes and approximately eightfold lower frequency (Sara et al., 2005). The higher fraction of HEK cells with mEPSCs, higher mEPSC frequency, and larger amplitude we observed with neuroligin 1, PSD-95, GluA2, and stargazin (Fig. 1 B and Fig. 2 C) could reflect either the presence of PSD-95 and stargazin in our study, or a greater efficacy of neuroligin-neuroligin signaling (Nam and Chen, 2005; Varoqueaux et al., 2006), or the younger neurons and different species (rat) used by Biederer et al. (2002) and Sara et al. (2005).

Our results support the view that synapses on heterologous cells recapitulate many aspects of native synaptic function (Fu et al., 2003; Sara et al., 2005). mEPSCs in HEK cells had greater amplitudes and more rapid rises and decays. Speed is generally viewed as an important adaptive property in synaptic transmission (Jackson, 1989). From this perspective, the present results suggest that the performance of synapses on HEK cells exceeds that of synapses on neurons. Rapid synaptic transmission depends on narrow synaptic clefts and close alignment between pre- and postsynaptic elements. The present results indicate that neuron-HEK cell synapses recapitulate these structural features. If detailed structural studies of the molecular organization of synapses between neurons (Biederer et al., 2017) can be complemented with comparable studies in heterologous synapses, we may be in a position to attempt more detailed interpretations of the quantitative differences in functional dynamics.

Quantal variations

With receptors in excess, mEPSC area should reflect the quantity of glutamate released per vesicle (Liu et al., 1999; Hanse and Gustafsson, 2001; Franks et al., 2003), which depends on vesicle size (Bekkers et al., 1990; Zhang et al., 1998; Bruns et al., 2000; Karunanithi et al., 2002) and intravesicular concentration (Song et al., 1997; Wojcik et al., 2004; Wilson et al., 2005; Wu et al., 2007). The similar areas (Fig. 2 C) and distributions of (area)^{1/3} (Fig. 3, E and F) suggest that vesicles release the same amount of glutamate from synapses on neurons and on HEK

cells. A higher receptor density in HEK cells would then reduce the radial distance within the synaptic cleft that glutamate diffuses before binding to receptors, thus making the rise more rapid and synchronizing channel opening to give a higher amplitude (Fig. 2 C). A higher subsynaptic receptor density could simply reflect stronger GluA2 expression in HEK cells, or better recruitment due to higher expression of PSD-95 and/or stargazin (Bats et al., 2007; MacGillavry et al., 2013), or endogenous N-cadherin (Inada et al., 2016).

The CVs of amplitude and decay time were significantly higher for HEK cell mEPSCs than 18-DIV neuronal mEPSCs, but the CV of rise rate was significantly lower (Fig. 2 D). Since glutamate receptors in neurons show considerable variation in subunit composition (Wenthold et al., 1996; Lu et al., 2009), the comparison presented here suggests that this variation has relatively little impact on the shape and variance of mEPSCs in neurons. The greater CV for amplitude and decay time in HEK cells is consistent with heterogeneity of receptor density. Receptor density will impact mEPSC amplitude and decay directly, and packing synaptic inputs at a higher density will reduce the distance between contacts to enhance transmitter spillover and further increase variations (Nielsen et al., 2004; Sargent et al., 2005). By contrast, the CV of mEPSC rise rate was lower in HEK cells (Fig. 2 D), and this may reflect the uniform absence of dendritic filtering. mEPSC onset in HEK cells may depend on less variable factors such as fusion pore flux.

Receptor contributions

Q→R edited flop is the most abundant GluA2 form in the brain (Wright and Vissel, 2012). We used this subunit to generate postsynaptic glutamate receptors, and with only this subunit expressed in HEK cells, their synapses will have a uniform population of homomeric GluA2 receptors. The majority of AMPA receptors in adult hippocampal neurons are GluA1/GluA2 and GluA2/GluA3 heteromers (Wenthold et al., 1996; Lu et al., 2009). Although GluA1 is more abundant in hippocampal neurons (Craig et al., 1993), homomeric GluA2 receptors target synaptic contacts (Shi et al., 2001). Ablating GluA1 and GluA3 produces a large reduction in evoked synaptic AMPA receptor-mediated synaptic currents, but the remaining homomeric GluA2 receptors produce mEPSC with amplitudes only ~15% lower than controls, with decays that are ~30% longer (Lu et al., 2009). By contrast, decays were approximately twofold faster in HEK cells than in neurons (Fig. 2 C), suggesting an influence of factors other than GluA subunits. Aniracetam increased the area and amplitude of mEPSCs in neuronal synapses (Chiang et al., 2018), and the different actions seen here in HEK cell mEPSCs (Fig. 5) are likely due to receptor differences (Johansen et al., 1995).

Our kinetic model was drawn from experiments with the same receptor used here, Q→R GluA2 flop, and the same cells, HEK293 (Krampfl et al., 2002). Although a single exponential fitted the decays of individual events (Fig. 2 A), averaged mEPSCs reduced the noise level to reveal a bi-exponential decay that diverged from the simulated mEPSC (Fig. 7). A likely source for these disparities is the accessory protein stargazin, which was not employed by Krampfl et al. (2002). Stargazin modulates

AMPA receptors, including those formed from GluA2 (Priel et al., 2005; Tomita et al., 2005; Carrillo et al., 2020), and has been proposed to promote bi-exponential decays in excitatory synaptic currents (Zhang et al., 2006). Thus, cocultures provide a system for testing how molecular variations in the postsynaptic apparatus control the mEPSC time course.

Dendritic filtering on mEPSCs

The impact of dendrites on synaptic responses is well established (Rall, 1967; Jack and Redman, 1971; Rall, 1989). Dendritic filtering has been shown to affect mEPSCs and contribute to their variance, but considerable variance remains after correction for cable effects (Ulrich and Lüscher, 1993; Bekkers and Stevens, 1996). The comparison of mEPSCs in neurons and morphologically compact HEK cells (Fig. 1 A) provides a new and direct test of the role of electrotonic conduction. The slower rises and decays in neuronal mEPSCs (Fig. 2 C) qualitatively agree with expectations of cable filtering. However, the higher CVs of amplitude and decay time in HEK cells than in neurons (Fig. 2 D) support the idea of other significant contributions to variance (Ulrich and Lüscher, 1993; Bekkers and Stevens, 1996). Simulations of the effect of dendritic filtering over a range of dendritic locations (Fig. 4) accounted for the slower rate of rise and suggested that inputs are relatively proximal ($X = 0.1$). However, the simulations failed to provide a full account for the slower decay. Our modeling of cable effects indicated that the mEPSCs recorded in neurons could not be generated by electrotonic distortion of synaptic inputs of the form recorded in HEK cells (Fig. 4, B and C). These results suggest that electrotonic conduction slows the onset of neuronal mEPSCs, while receptors, auxiliary subunits, and electrotonic conduction work together to shape the decay.

Fusion pore effects

Flux through the fusion pore shapes the mEPSC rise and is thought to set up a transient steady state in glutamate concentration balanced by radial diffusion away from the release site (Khanin et al., 1994; Clements, 1996; Stiles et al., 1996; Chiang et al., 2018). The role of fusion pore flux was tested in neuron-HEK cell synapses with Syb2 transmembrane domain mutations. As found previously in neuron-neuron synapses (Chiang et al., 2018), incorporating a bulky tryptophan side chain into position 101 or both 101 and 103 reduced the mEPSC rise rate and slowed the decay (Fig. 6). These results are consistent with the role of Syb2 in synaptic (Chiang et al., 2018) and endocrine (Chang et al., 2015) fusion pores. A model of the WT HEK cell mEPSC recapitulated the concomitant reduction in amplitude and rise rate reasonably well by adjusting only one parameter, the fusion pore flux (Fig. 7). These results thus support a model of the initial fusion pore lined by SNARE protein transmembrane domains (Chang et al., 2017). The HEK cell coculture yielded clearer results than pure neuronal cultures, suggesting that eliminating dendritic filtering can improve such studies.

Conclusions

A detailed comparison of mEPSCs in neurons and heterologous HEK cells permitted an evaluation of a number of important

factors that contribute to the time course of synaptic transmission. This study strengthened the view that synapses on heterologous cells recapitulate native synaptic function with high fidelity but also revealed subtle differences. Receptor properties, fusion pores, and dendritic filtering impact the shapes of mEPSCs in distinct ways. Neuron-HEK cell cocultures offer a system for investigation of mEPSCs mediated by a postsynaptic apparatus with a defined molecular composition. The high resolution afforded by this system will be useful in further studies to probe the molecular mechanisms of the distinct steps that occur sequentially during synaptic transmission.

Acknowledgments

Jeanne M. Nerbonne served as editor.

We thank Dr. Lu Chen for providing constructs encoding neuroligin 1, stargazin-GFP, PSD-95, and GFP-GluA2. We thank Mazdak Bradburry for advice on cocultures, and Che-Wei Chang and Vasanthi Jayaraman for helpful discussions and comments.

This study was supported by National Institutes of Health grant NS044057.

The authors declare no competing financial interests.

Author contributions: C.-W. Chiang designed the experiments, generated DNA constructs, prepared the cultures and viral vectors, performed the patch clamp recordings, analyzed data, and wrote the paper. W.-C. Shu assisted in interpretations, analysis, and writing. J. Wan and B.A. Weaver generated DNA constructs. M.B. Jackson designed experiments, analyzed data, and wrote the paper.

Submitted: 11 December 2020

Revised: 26 January 2021

Accepted: 23 February 2021

References

- Andreae, L.C., N.B. Fredj, and J. Burrone. 2012. Independent vesicle pools underlie different modes of release during neuronal development. *J. Neurosci.* 32:1867–1874. <https://doi.org/10.1523/JNEUROSCI.5181-11.2012>
- Bao, H., D. Das, N.A. Courtney, Y. Jiang, J.S. Briguglio, X. Lou, D. Roston, Q. Cui, B. Chanda, and E.R. Chapman. 2018. Dynamics and number of trans-SNARE complexes determine nascent fusion pore properties. *Nature.* 554:260–263. <https://doi.org/10.1038/nature25481>
- Bats, C., L. Groc, and D. Choquet. 2007. The interaction between Stargazin and PSD-95 regulates AMPA receptor surface trafficking. *Neuron.* 53:719–734. <https://doi.org/10.1016/j.neuron.2007.01.030>
- Bekkers, J.M. 1994. Quantal analysis of synaptic transmission in the central nervous system. *Curr. Opin. Neurobiol.* 4:360–365. [https://doi.org/10.1016/0959-4388\(94\)90097-3](https://doi.org/10.1016/0959-4388(94)90097-3)
- Bekkers, J.M., and C.F. Stevens. 1995. Quantal analysis of EPSCs recorded from small numbers of synapses in hippocampal cultures. *J. Neurophysiol.* 73:1145–1156. <https://doi.org/10.1152/jn.1995.73.3.1145>
- Bekkers, J.M., and C.F. Stevens. 1996. Cable properties of cultured hippocampal neurons determined from sucrose-evoked miniature EPSCs. *J. Neurophysiol.* 75:1250–1255. <https://doi.org/10.1152/jn.1996.75.3.1250>
- Bekkers, J.M., G.B. Richerson, and C.F. Stevens. 1990. Origin of variability in quantal size in cultured hippocampal neurons and hippocampal slices. *Proc. Natl. Acad. Sci. USA.* 87:5359–5362. <https://doi.org/10.1073/pnas.87.14.5359>
- Biederer, T., Y. Sara, M. Mozhayeva, D. Atasoy, X. Liu, E.T. Kavalali, and T.C. Südhof. 2002. SynCAM, a synaptic adhesion molecule that drives synapse assembly. *Science.* 297:1525–1531. <https://doi.org/10.1126/science.1072356>

- Biederer, T., P.S. Kaeser, and T.A. Blanpied. 2017. Transcellular Nanoalignment of Synaptic Function. *Neuron*. 96:680–696. <https://doi.org/10.1016/j.neuron.2017.10.006>
- Brenowitz, S., and L.O. Trussell. 2001. Minimizing synaptic depression by control of release probability. *J. Neurosci.* 21:1857–1867. <https://doi.org/10.1523/JNEUROSCI.21-06-01857.2001>
- Bruns, D., D. Riedel, J. Klingauf, and R. Jahn. 2000. Quantal release of serotonin. *Neuron*. 28:205–220. [https://doi.org/10.1016/S0896-6273\(00\)00097-0](https://doi.org/10.1016/S0896-6273(00)00097-0)
- Carrillo, E., N.K. Bhatia, A.M. Akimzhanov, and V. Jayaraman. 2020. Activity Dependent Inhibition of AMPA Receptors by Zn²⁺. *J. Neurosci.* 40: 8629–8636. <https://doi.org/10.1523/JNEUROSCI.1481-20.2020>
- Chang, C.W., E. Hui, J. Bai, D. Bruns, E.R. Chapman, and M.B. Jackson. 2015. A structural role for the synaptobrevin 2 transmembrane domain in dense-core vesicle fusion pores. *J. Neurosci.* 35:5772–5780. <https://doi.org/10.1523/JNEUROSCI.3983-14.2015>
- Chang, C.W., C.W. Chiang, and M.B. Jackson. 2017. Fusion pores and their control of neurotransmitter and hormone release. *J. Gen. Physiol.* 149: 301–322. <https://doi.org/10.1085/jgp.201611724>
- Chen, L., D.M. Chetkovich, R.S. Petralia, N.T. Sweeney, Y. Kawasaki, R.J. Wenthold, D.S. Bredt, and R.A. Nicoll. 2000. Stargazin regulates synaptic targeting of AMPA receptors by two distinct mechanisms. *Nature*. 408:936–943. <https://doi.org/10.1038/35050030>
- Chiang, C.W., C.W. Chang, and M.B. Jackson. 2018. The Transmembrane Domain of Synaptobrevin Influences Neurotransmitter Flux through Synaptic Fusion Pores. *J. Neurosci.* 38:7179–7191. <https://doi.org/10.1523/JNEUROSCI.0721-18.2018>
- Clements, J.D. 1996. Transmitter timecourse in the synaptic cleft: its role in central synaptic function. *Trends Neurosci.* 19:163–171. [https://doi.org/10.1016/S0166-2236\(96\)10024-2](https://doi.org/10.1016/S0166-2236(96)10024-2)
- Craig, A.M., C.D. Blackstone, R.L. Haganir, and G. Banker. 1993. The distribution of glutamate receptors in cultured rat hippocampal neurons: postsynaptic clustering of AMPA-selective subunits. *Neuron*. 10: 1055–1068. [https://doi.org/10.1016/0896-6273\(93\)90054-U](https://doi.org/10.1016/0896-6273(93)90054-U)
- Dean, C., and T. Dresbach. 2006. Neuroligins and neuexins: linking cell adhesion, synapse formation and cognitive function. *Trends Neurosci.* 29:21–29. <https://doi.org/10.1016/j.tins.2005.11.003>
- Dean, C., F.G. Scholl, J. Choih, S. DeMaria, J. Berger, E. Isacoff, and P. Scheiffele. 2003. Neuexin mediates the assembly of presynaptic terminals. *Nat. Neurosci.* 6:708–716. <https://doi.org/10.1038/nrn1074>
- Dixon, C.L., Y. Zhang, and J.W. Lynch. 2015. Generation of Functional Inhibitory Synapses Incorporating Defined Combinations of GABA(A) or Glycine Receptor Subunits. *Front. Mol. Neurosci.* 8:80. <https://doi.org/10.3389/fnmol.2015.00080>
- Dong, N., J. Qi, and G. Chen. 2007. Molecular reconstitution of functional GABAergic synapses with expression of neuroligin-2 and GABAA receptors. *Mol. Cell. Neurosci.* 35:14–23. <https://doi.org/10.1016/j.mcn.2007.01.013>
- Finch, D.M., R.S. Fisher, and M.B. Jackson. 1990. Miniature excitatory synaptic currents in cultured hippocampal neurons. *Brain Res.* 518:257–268. [https://doi.org/10.1016/0006-8993\(90\)90978-K](https://doi.org/10.1016/0006-8993(90)90978-K)
- Franks, K.M., C.F. Stevens, and T.J. Sejnowski. 2003. Independent sources of quantal variability at single glutamatergic synapses. *J. Neurosci.* 23: 3186–3195. <https://doi.org/10.1523/JNEUROSCI.23-08-03186.2003>
- Fu, Z., P. Washbourne, P. Ortinski, and S. Vicini. 2003. Functional excitatory synapses in HEK293 cells expressing neuroligin and glutamate receptors. *J. Neurophysiol.* 90:3950–3957. <https://doi.org/10.1152/jn.00647.2003>
- Geiger, J.R., T. Melcher, D.S. Koh, B. Sakmann, P.H. Seeburg, P. Jonas, and H. Monyer. 1995. Relative abundance of subunit mRNAs determines gating and Ca²⁺ permeability of AMPA receptors in principal neurons and interneurons in rat CNS. *Neuron*. 15:193–204. [https://doi.org/10.1016/0896-6273\(95\)90076-4](https://doi.org/10.1016/0896-6273(95)90076-4)
- Guzman, R.E., Y.N. Schwarz, J. Rettig, and D. Bruns. 2010. SNARE force synchronizes synaptic vesicle fusion and controls the kinetics of quantal synaptic transmission. *J. Neurosci.* 30:10272–10281. <https://doi.org/10.1523/JNEUROSCI.1551-10.2010>
- Hanse, E., and B. Gustafsson. 2001. Quantal variability at glutamatergic synapses in area CA1 of the rat neonatal hippocampus. *J. Physiol.* 531: 467–480. <https://doi.org/10.1111/j.1469-7793.2001.04671.x>
- Inada, M., G. Izawa, W. Kobayashi, and M. Ozawa. 2016. 293 cells express both epithelial as well as mesenchymal cell adhesion molecules. *Int. J. Mol. Med.* 37:1521–1527. <https://doi.org/10.3892/ijmm.2016.2568>
- Isaacson, J.S., and R.A. Nicoll. 1991. Aniracetam reduces glutamate receptor desensitization and slows the decay of fast excitatory synaptic currents in the hippocampus. *Proc. Natl. Acad. Sci. USA.* 88:10936–10940. <https://doi.org/10.1073/pnas.88.23.10936>
- Ito, I., S. Tanabe, A. Kohda, and H. Sugiyama. 1990. Allosteric potentiation of quisqualate receptors by a nootropic drug aniracetam. *J. Physiol.* 424: 533–543. <https://doi.org/10.1113/jphysiol.1990.sp018081>
- Jack, J.J., and S.J. Redman. 1971. An electrical description of the motoneurone, and its application to the analysis of synaptic potentials. *J. Physiol.* 215: 321–352. <https://doi.org/10.1113/jphysiol.1971.sp009473>
- Jackson, M.B. 1989. Perfection of a synaptic receptor: kinetics and energetics of the acetylcholine receptor. *Proc. Natl. Acad. Sci. USA.* 86:2199–2203. <https://doi.org/10.1073/pnas.86.7.2199>
- Jackson, M.B. 2006. *Molecular and Cellular Biophysics*. Cambridge University Press, Cambridge, UK. 512 pp. <https://doi.org/10.1017/CBO9780511754869>
- Johansen, T.H., A. Chaudhary, and T.A. Verdoorn. 1995. Interactions among GYKI-52466, cyclothiazide, and aniracetam at recombinant AMPA and kainate receptors. *Mol. Pharmacol.* 48:946–955.
- Karunanithi, S., L. Marin, K. Wong, and H.L. Atwood. 2002. Quantal size and variation determined by vesicle size in normal and mutant *Drosophila* glutamatergic synapses. *J. Neurosci.* 22:10267–10276. <https://doi.org/10.1523/JNEUROSCI.22-23-10267.2002>
- Khanin, R., H. Parnas, and L. Segel. 1994. Diffusion cannot govern the discharge of neurotransmitter in fast synapses. *Biophys. J.* 67:966–972. [https://doi.org/10.1016/S0006-3495\(94\)80562-4](https://doi.org/10.1016/S0006-3495(94)80562-4)
- Krampfl, K., F. Schlesinger, A. Zörner, M. Kappler, R. Dengler, and J. Bufler. 2002. Control of kinetic properties of GluR2 flop AMPA-type channels: impact of R/G nuclear editing. *Eur. J. Neurosci.* 15:51–62. <https://doi.org/10.1046/j.0953-816x.2001.01841.x>
- Lawrence, J.J., S. Brenowitz, and L.O. Trussell. 2003. The mechanism of action of aniracetam at synaptic alpha-amino-3-hydroxy-5-methyl-4-isoxazolepropionic acid (AMPA) receptors: indirect and direct effects on desensitization. *Mol. Pharmacol.* 64:269–278. <https://doi.org/10.1124/mol.64.2.269>
- Lindau, M., and G. Alvarez de Toledo. 2003. The fusion pore. *Biochim. Biophys. Acta.* 1641:167–173. [https://doi.org/10.1016/S0167-4889\(03\)00085-5](https://doi.org/10.1016/S0167-4889(03)00085-5)
- Lisman, J.E., S. Raghavachari, and R.W. Tsien. 2007. The sequence of events that underlie quantal transmission at central glutamatergic synapses. *Nat. Rev. Neurosci.* 8:597–609. <https://doi.org/10.1038/nrn2191>
- Liu, G., S. Choi, and R.W. Tsien. 1999. Variability of neurotransmitter concentration and nonsaturation of postsynaptic AMPA receptors at synapses in hippocampal cultures and slices. *Neuron*. 22:395–409. [https://doi.org/10.1016/S0896-6273\(00\)81099-5](https://doi.org/10.1016/S0896-6273(00)81099-5)
- Lomeli, H., J. Mosbacher, T. Melcher, T. Höger, J.R. Geiger, T. Kuner, H. Monyer, M. Higuchi, A. Bach, and P.H. Seeburg. 1994. Control of kinetic properties of AMPA receptor channels by nuclear RNA editing. *Science*. 266:1709–1713. <https://doi.org/10.1126/science.7992055>
- Lu, W., Y. Shi, A.C. Jackson, K. Bjorgan, M.J. Doring, R. Sprengel, P.H. Seeburg, and R.A. Nicoll. 2009. Subunit composition of synaptic AMPA receptors revealed by a single-cell genetic approach. *Neuron*. 62: 254–268. <https://doi.org/10.1016/j.neuron.2009.02.027>
- MacGillavry, H.D., Y. Song, S. Raghavachari, and T.A. Blanpied. 2013. Nanoscale scaffolding domains within the postsynaptic density concentrate synaptic AMPA receptors. *Neuron*. 78:615–622. <https://doi.org/10.1016/j.neuron.2013.03.009>
- Mozhayeva, M.G., Y. Sara, X. Liu, and E.T. Kavalali. 2002. Development of vesicle pools during maturation of hippocampal synapses. *J. Neurosci.* 22:654–665. <https://doi.org/10.1523/JNEUROSCI.22-03-00654.2002>
- Nam, C.I., and L. Chen. 2005. Postsynaptic assembly induced by neuroligin-neuroligin interaction and neurotransmitter. *Proc. Natl. Acad. Sci. USA.* 102:6137–6142. <https://doi.org/10.1073/pnas.0502038102>
- Nielsen, T.A., D.A. DiGregorio, and R.A. Silver. 2004. Modulation of glutamate mobility reveals the mechanism underlying slow-rising AMPAR EPSCs and the diffusion coefficient in the synaptic cleft. *Neuron*. 42: 757–771. <https://doi.org/10.1016/j.neuron.2004.04.003>
- Pawlu, C., A. DiAntonio, and M. Heckmann. 2004. Postfusional control of quantal current shape. *Neuron*. 42:607–618. [https://doi.org/10.1016/S0896-6273\(04\)00269-7](https://doi.org/10.1016/S0896-6273(04)00269-7)
- Priel, A., A. Kollerker, G. Ayalon, M. Gillor, P. Osten, and Y. Stern-Bach. 2005. Stargazin reduces desensitization and slows deactivation of the AMPA-type glutamate receptors. *J. Neurosci.* 25:2682–2686. <https://doi.org/10.1523/JNEUROSCI.4834-04.2005>
- Rall, W. 1967. Distinguishing theoretical synaptic potentials computed for different soma-dendritic distributions of synaptic input. *J. Neurophysiol.* 30:1138–1168. <https://doi.org/10.1152/jn.1967.30.5.1138>
- Rall, W. 1969. Time constants and electrotonic length of membrane cylinders and neurons. *Biophys. J.* 9:1483–1508. [https://doi.org/10.1016/S0006-3495\(69\)86467-2](https://doi.org/10.1016/S0006-3495(69)86467-2)

- Rall, W. 1989. Cable theory for dendritic neurons. In *Methods in Neuronal Modeling*. C.K.I. Segev, editor. MIT Press, Cambridge. 9–62.
- Rall, W., R.E. Burke, T.G. Smith, P.G. Nelson, and K. Frank. 1967. Dendritic location of synapses and possible mechanisms for the monosynaptic EPSP in motoneurons. *J. Neurophysiol.* 30:1169–1193. <https://doi.org/10.1152/jn.1967.30.5.1169>
- Rothman, J.S., and R.A. Silver. 2018. NeuroMatic: An Integrated Open-Source Software Toolkit for Acquisition, Analysis and Simulation of Electrophysiological Data. *Front. Neuroinform.* 12:14. <https://doi.org/10.3389/fninf.2018.00014>
- Sabatini, B.L., and W.G. Regehr. 1999. Timing of synaptic transmission. *Annu. Rev. Physiol.* 61:521–542. <https://doi.org/10.1146/annurev.physiol.61.1.521>
- Sara, Y., T. Biederer, D. Atasoy, A. Chubykin, M.G. Mozhayeva, T.C. Südhof, and E.T. Kavalali. 2005. Selective capability of SynCAM and neuroligin for functional synapse assembly. *J. Neurosci.* 25:260–270. <https://doi.org/10.1523/JNEUROSCI.3165-04.2005>
- Sargent, P.B., C. Saviane, T.A. Nielsen, D.A. DiGregorio, and R.A. Silver. 2005. Rapid vesicular release, quantal variability, and spillover contribute to the precision and reliability of transmission at a glomerular synapse. *J. Neurosci.* 25:8173–8187. <https://doi.org/10.1523/JNEUROSCI.2051-05.2005>
- Scanziani, M., M. Capogna, B.H. Gähwiler, and S.M. Thompson. 1992. Presynaptic inhibition of miniature excitatory synaptic currents by baclofen and adenosine in the hippocampus. *Neuron.* 9:919–927. [https://doi.org/10.1016/0896-6273\(92\)90244-8](https://doi.org/10.1016/0896-6273(92)90244-8)
- Scheiffele, P., J. Fan, J. Choih, R. Fetter, and T. Serafini. 2000. Neuroligin expressed in nonneuronal cells triggers presynaptic development in contacting axons. *Cell.* 101:657–669. [https://doi.org/10.1016/S0092-8674\(00\)80877-6](https://doi.org/10.1016/S0092-8674(00)80877-6)
- Schnell, E., M. Sizemore, S. Karimzadegan, L. Chen, D.S. Bredt, and R.A. Nicoll. 2002. Direct interactions between PSD-95 and stargazin control synaptic AMPA receptor number. *Proc. Natl. Acad. Sci. USA.* 99:13902–13907. <https://doi.org/10.1073/pnas.172511199>
- Shi, S., Y. Hayashi, J.A. Esteban, and R. Malinow. 2001. Subunit-specific rules governing AMPA receptor trafficking to synapses in hippocampal pyramidal neurons. *Cell.* 105:331–343. [https://doi.org/10.1016/S0092-8674\(01\)00321-X](https://doi.org/10.1016/S0092-8674(01)00321-X)
- Song, H., G. Ming, E. Fon, E. Bellocchio, R.H. Edwards, and M. Poo. 1997. Expression of a putative vesicular acetylcholine transporter facilitates quantal transmitter packaging. *Neuron.* 18:815–826. [https://doi.org/10.1016/S0896-6273\(00\)80320-7](https://doi.org/10.1016/S0896-6273(00)80320-7)
- Stiles, J.R., D. Van Helden, T.M. Bartol Jr., E.E. Salpeter, and M.M. Salpeter. 1996. Miniature endplate current rise times less than 100 microseconds from improved dual recordings can be modeled with passive acetylcholine diffusion from a synaptic vesicle. *Proc. Natl. Acad. Sci. USA.* 93:5747–5752. <https://doi.org/10.1073/pnas.93.12.5747>
- Tomita, S., H. Adesnik, M. Sekiguchi, W. Zhang, K. Wada, J.R. Howe, R.A. Nicoll, and D.S. Bredt. 2005. Stargazin modulates AMPA receptor gating and trafficking by distinct domains. *Nature.* 435:1052–1058. <https://doi.org/10.1038/nature03624>
- Ulrich, D., and H.R. Lüscher. 1993. Miniature excitatory synaptic currents corrected for dendritic cable properties reveal quantal size and variance. *J. Neurophysiol.* 69:1769–1773. <https://doi.org/10.1152/jn.1993.69.5.1769>
- Varoqueaux, F., G. Aramuni, R.L. Rawson, R. Mohrmann, M. Missler, K. Gottmann, W. Zhang, T.C. Südhof, and N. Brose. 2006. Neuroligins determine synapse maturation and function. *Neuron.* 51:741–754. <https://doi.org/10.1016/j.neuron.2006.09.003>
- Vyklicky, L. Jr., D.K. Patneau, and M.L. Mayer. 1991. Modulation of excitatory synaptic transmission by drugs that reduce desensitization at AMPA/kainate receptors. *Neuron.* 7:971–984. [https://doi.org/10.1016/0896-6273\(91\)90342-W](https://doi.org/10.1016/0896-6273(91)90342-W)
- Wenthold, R.J., R.S. Petralia, I.I. Blahos J, and A.S. Niedzielski. 1996. Evidence for multiple AMPA receptor complexes in hippocampal CA1/CA2 neurons. *J. Neurosci.* 16:1982–1989. <https://doi.org/10.1523/JNEUROSCI.16-06-01982.1996>
- Wilson, N.R., J. Kang, E.V. Hueske, T. Leung, H. Varoqui, J.G. Murnick, J.D. Erickson, and G. Liu. 2005. Presynaptic regulation of quantal size by the vesicular glutamate transporter VGLUT1. *J. Neurosci.* 25:6221–6234. <https://doi.org/10.1523/JNEUROSCI.3003-04.2005>
- Wojcik, S.M., J.S. Rhee, E. Herzog, A. Sigler, R. Jahn, S. Takamori, N. Brose, and C. Rosenmund. 2004. An essential role for vesicular glutamate transporter 1 (VGLUT1) in postnatal development and control of quantal size. *Proc. Natl. Acad. Sci. USA.* 101:7158–7163. <https://doi.org/10.1073/pnas.0401764101>
- Wright, A., and B. Vissel. 2012. The essential role of AMPA receptor GluR2 subunit RNA editing in the normal and diseased brain. *Front. Mol. Neurosci.* 5:34. <https://doi.org/10.3389/fnmol.2012.00034>
- Wu, X.S., L. Xue, R. Mohan, K. Paradiso, K.D. Gillis, and L.G. Wu. 2007. The origin of quantal size variation: vesicular glutamate concentration plays a significant role. *J. Neurosci.* 27:3046–3056. <https://doi.org/10.1523/JNEUROSCI.4415-06.2007>
- Zhang, B., Y.H. Koh, R.B. Beckstead, V. Budnik, B. Ganetzky, and H.J. Bellen. 1998. Synaptic vesicle size and number are regulated by a clathrin adaptor protein required for endocytosis. *Neuron.* 21:1465–1475. [https://doi.org/10.1016/S0896-6273\(00\)80664-9](https://doi.org/10.1016/S0896-6273(00)80664-9)
- Zhang, W., A. Robert, S.B. Vogensen, and J.R. Howe. 2006. The relationship between agonist potency and AMPA receptor kinetics. *Biophys. J.* 91:1336–1346. <https://doi.org/10.1529/biophysj.106.084426>